photonics

MDPI

Article

Interference Measurements Across Vacuum and Atmospheric Environments for Characterization of Space-Borne Telescope

Yi-Kai Huang [1,2] and Cheng-Huan Chen [1,*]

[1] Department of Photonics, College of Electrical and Computer Engineering, National Yang Ming Chiao Tung University, 1001 University Road, Hsinchu 300, Taiwan; bkhuang@tasa.org.tw
[2] Optical Payload Division, Taiwan Space Agency, 8F, 9 Prosperity 1st Road, Hsinchu Science Park, Hsinchu 300, Taiwan
* Correspondence: chhuchen@nycu.edu.tw

Abstract: A space-borne telescope is used for Earth observation at about 500 km above sea level in the thermosphere where the air density is very low and the temperature increases significantly during daytime. If the telescopes are aligned and characterized on the ground with standard temperature and pressure (STP) conditions, different from that of the thermosphere, their performance could drift during their mission. Therefore, they are usually placed in a thermal vacuum chamber during ground testing in order to verify the system can perform well and withstand the harsh environment such as a high vacuum level and large temperature variations before being launched. Nevertheless, it remains a challenge to build up an in situ optical measurement system for a large aperture telescope in a thermal vacuum chamber due to the finite internal space of the chamber, limited aperture size of the vacuum view port and thermal dissipation problem of the measuring instruments. In this paper, a novel architecture of an interferometer whose light path travels across a vacuum chamber and an atmospheric environment has been proposed to resolve all of these technical issues. The major feature of the architecture is the diverger lens being located within the vacuum chamber, leaving the rest of the interferometer outside. The variation of the interference fringe due to the relocation of the diverger lens has been investigated with optical simulations and the solutions for compensation have also been proposed. Together with a specific alignment procedure for the proposed architecture, the interferogram has been successfully acquired from a prototype testbed.

Keywords: space-borne telescope; interferometry; thermal vacuum test

Citation: Huang, Y.-K.; Chen, C.-H. Interference Measurements Across Vacuum and Atmospheric Environments for Characterization of Space-Borne Telescope. *Photonics* **2024**, *11*, 1105. https://doi.org/10.3390/photonics11121105

Received: 19 October 2024
Revised: 19 November 2024
Accepted: 20 November 2024
Published: 22 November 2024

1. Introduction

For those optical systems applied for space missions, the opto-mechanical design is a decisive factor in the final optical performance, which is related to not only the surface error control of the optics while the optical system suffers from its working environment but also for maintaining the stability of the optical elements in the mechanical structure that will allow the optical system to perform correctly. Due to the mass budget of a space mission, the mechanical structures are usually made of carbon fiber reinforced polymer (CFRP) materials due to their lightweight. However, CFRP materials absorb water from humid environments on Earth and desorb that moisture in vacuum, which may cause contamination issues as well as dimensional changes of sensitive components [1]. Moreover, for a low Earth orbit, the satellite would rotate around the Sun with the Earth and its surface temperature is about ±100 °C, which would produce thermal deformation behavior of the telescope structure and eventually lead to positioning errors of the optics. As a result, a technique for monitoring the optical performance variations due to dimensional changes in vacuum become crucial.

Elaine et al. illustrated the lesson learned for the TopSat camera, describing the relationship between the optical tolerance and opto-mechanical design and how they

conducted the integration and testing for their telescope. The wavefront error (WFE) measurement was conducted in standard temperature and pressure (STP) conditions. After that, a thermal vacuum test for thermal model validation was conducted without measuring the optical performance [2]. Christof et al. demonstrated optical thermal vacuum testing for a near infrared spectrometer and photometer (NISP), which is one of the back-end instruments in an Euclidean space telescope with a small aperture size. The NISP was placed inside the chamber with the optical fiber light source on its focus. A high-quality cassegrain reflector with the same f-number of 20 as that of the main telescope system of the Euclid and Shack–Hartmann wavefront sensor (SHWFS) were set up out of the vacuum chamber. They observed the overall WFE variation under space operating conditions within a cryostat with the wavefront sensor [3]. In order to validate the optical performance for the whole Euclidean space telescope with its 1.2 m aperture optical system, a Belgium company (AMOS) built up a 1.4 m aperture collimator as an infinite object simulator to reproduce the orbit observation condition. Both the collimator and Euclid space telescope were placed inside a giant vacuum chamber. The collimator projected test sources with a collimated beam into the telescope and the test beam eventually focused on the image sensor of the telescope with signal readout just like the Euclid telescope was observing an infinite distance star in space [4,5].

As stated above, space optical systems would surely be tested in a thermal vacuum chamber and the engineers may attempt to realize how their system acts in such an extreme environment by implementing different kinds of measuring setups inside the chamber. Nevertheless, the vast majority of measurement instruments cannot operate correctly in vacuum because of the thermal dissipation problem and the material outgassing issues, which makes it difficult to place instruments in such a chamber. Additionally, due to the internal space limitations of a chamber, it is not easy to achieve the full test architecture like the Euclid with a collimator and telescope inside the chamber, which could only allow a part of the optics to be tested in a thermal vacuum circumstance. For an optical system already equipped with an image sensor, it may need further adjustment or reassembly if there is any optical performance degradation occurring during the test. Therefore, an interferometer architecture was proposed with the light path across the vacuum and an STP environment that could acquire the focus variation range and estimate the defocus margin of the telescope in advance.

2. Interferometer Architecture with Light Path Across Vacuum Chamber and STP Environment

The test object is a space-borne catadioptric telescope that was designed to conduct an Earth observation mission on a 500–600 km Sun-synchronous orbit and it could provide a multi-spectral image with 1 m resolution [6]. The telescope consists of a 40 cm diameter primary mirror (M1), a 14 cm diameter secondary mirror (M2) and a 4 lenses corrector module. The two mirrors are connected by a CFRP tube structure, which is a major source of defocus on the focal plane, as shown in Figure 1.

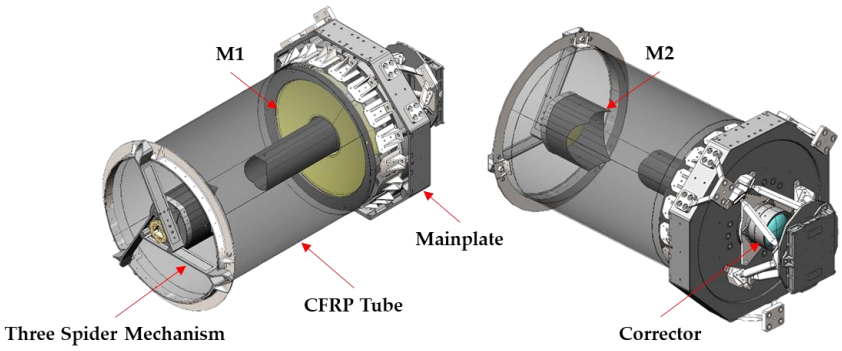

Figure 1. Opto-mechanical design of the space-borne catadioptric telescope.

The vacuum chamber in our facility is 2 m in diameter and 2.5 m in depth, equipped with a 25 cm diameter vacuum view port and its size is much smaller than the aperture of the telescope. The vacuum view port is the only transparent portion of the vacuum chamber, which can not only be used as the optical interface between the vacuum and the STP environment but also be featured as the transmission flat in the optical path. It is a dual-surface flat piece made of fused silica with 10 mm thickness and its surface flatness is better than $\lambda/10$. In order to observe the optical performance of telescope in thermal vacuum conditions and consider the size restriction of the chamber, an in situ double pass interferometry setup with a Twyman–Green interferometer was chosen, which could let us know the WFE variation and focus change while the telescope suffers from a high vacuum level and thermal cycling with large temperature differences.

However, the commercial interferometer could not operate correctly in vacuum because of the thermal dissipation issue, which would damage the interferometer itself, and the material outgassing issues, which may cause contamination of the test optics. Therefore, an idea of separating the diverger lens from the interferometer was proposed, which means only the diverger lens would be placed inside the chamber as shown in Figure 2. A collimated laser beam (He–Ne laser 632.8 nm) coming from the interferometer penetrated the vacuum view port and then was focused by the diverger lens on the focal plane simulator (FPS) with a pinhole. After passing through the corrector lens and being reflected by the M2 and M1 sequentially, it becomes collimatedly incident onto the auto collimation flat mirror. The auto collimation flat mirror was placed behind the M2, which would reflect the collimated beam then return to the telescope and interferometer by following the original optical path. Finally, the interferogram could be obtained with the superposition of the object beam from the telescope and the reference beam from the reference mirror on the detector of the interferometer.

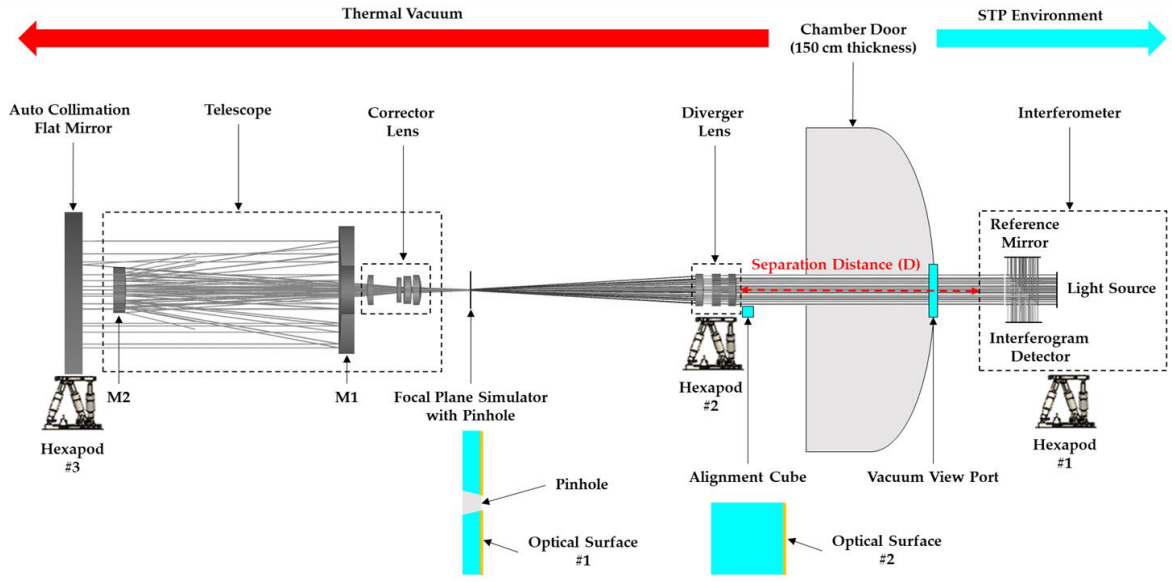

Figure 2. Double pass interferometry setup across thermal vacuum chamber and STP environment.

The feasibility test of diverger lens separation was conducted with the vacuum view port involved as illustrated in Figure 3a and it could successfully acquire the WFE result for the test optics on the premise that the diverger lens was well aligned with interferometer as shown in Figure 3b. Furthermore, for the double pass interferometry, in order to acquire the correct wavefront error result of the test telescope, it is essential to extract the wavefront error attributed by others, including the interferometer, vacuum view port, diverger lens, and auto collimation flat mirror, which is called the bias of measurement setup. Therefore, the WFE result of Figure 3b could also represent the bias map, which would be set as the reference during the actual measurement by the telescope.

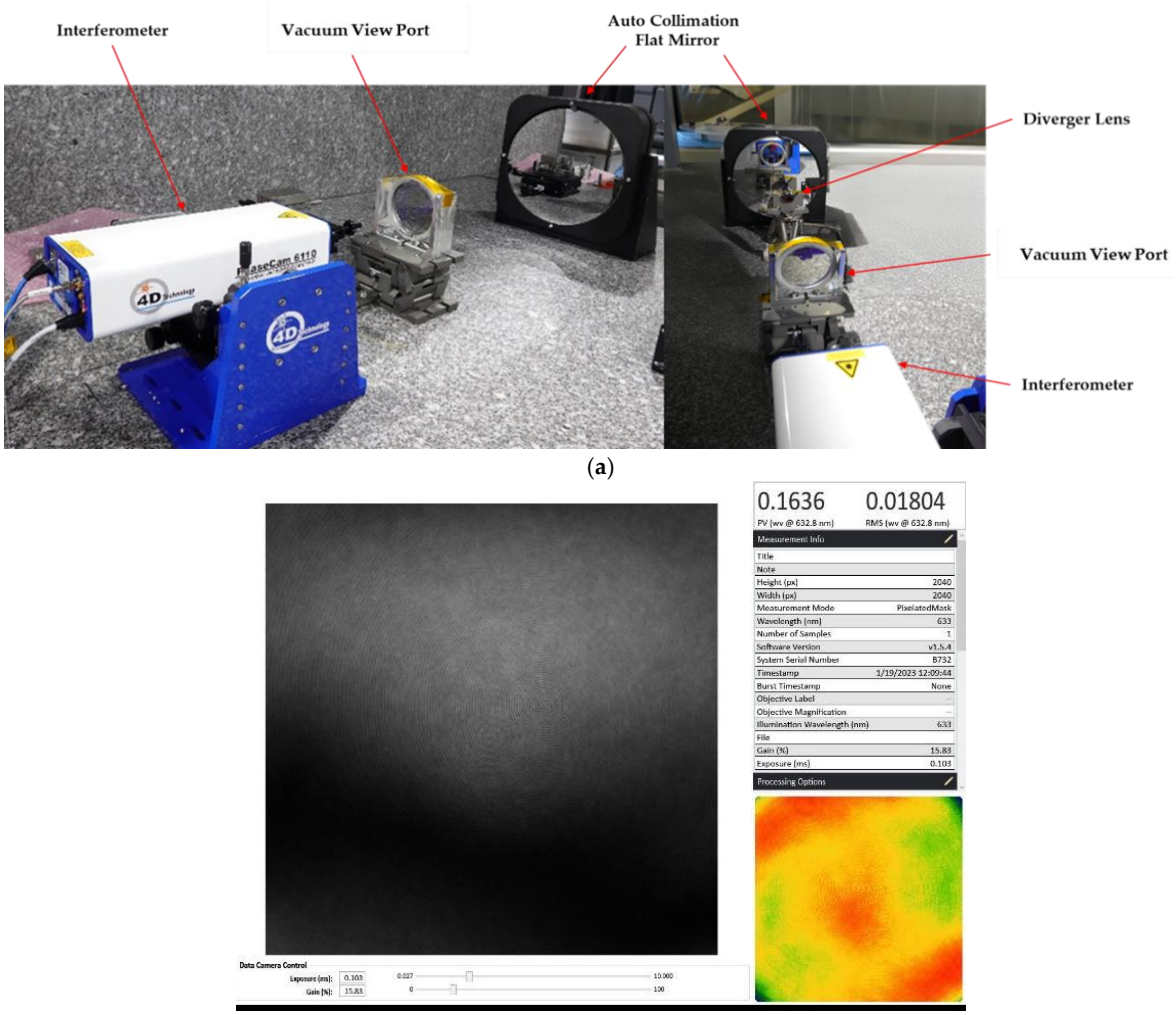

Figure 3. Feasibility test of separating the diverger lens from the interferometer. (**a**) Feasibility test for bias measurement, which includes the interferometer, vacuum view port, diverger lens and auto collimation flat mirror with cat's eye architecture. (**b**) WFE result of bias measurement.

3. Issues of Interference Fringe Degradation and Solutions for Compensation

After the success of the feasibility test, the first obstacle showed up, which is related to the long separation distance of the diverger lens and interferometer. Figure 2 illustrates the separation distance D of 150 cm in the actual measurement setup due to the thickness of the chamber door. From the viewpoint of the optical path, the extension of separation distance D should not be a problem in this double pass setup, which should be able to acquire the correct WFE result after the alignment work being accomplished. However, when increasing the separation distance D from the nominal value of 7 cm to the required separation distance of 150 cm, the interference fringe blurred out, which in turn affected the construction of the WFE map, as shown in Figure 4.

In order to investigate the cause of the abnormal interferogram, the Advanced Systems Analysis Program (ASAP) software (Version 6.7) was adopted to simulate the interference fringes while considering the diffraction effect from the coherent measuring system [7,8]. The ASAP is an optical engineering software used to simulate the straylight of optical systems by the non-sequential ray tracing with coherent as well as incoherent light sources. Figure 5 shows the double pass simulation model in ASAP where the color facets represent different surface properties. The yellow, blue and gray color present the reflective, transmit and absorb surfaces, respectively. The whole interferometry system comprises a diverger lens module, a reference mirror, a light source at 632.8 nm with 100 lm flux, and an

interferogram detector with 500 × 500 pixels. The diverger lens consists of three spherical lens elements as an aberration free module in the interferometric light path with the separation distance D from the interferometer. A focal plane simulator (FPS) with a 1 mm diameter pinhole, which is used to block the ghost fringe reflected by the corrector lens of the telescope while conducting the double pass interferometry, is located at the focal point of the diverger lens and image plane of the telescope. The three spider mechanisms for supporting the M2 are also included in the model because they are within the illumination area and could introduce a diffraction effect [9].

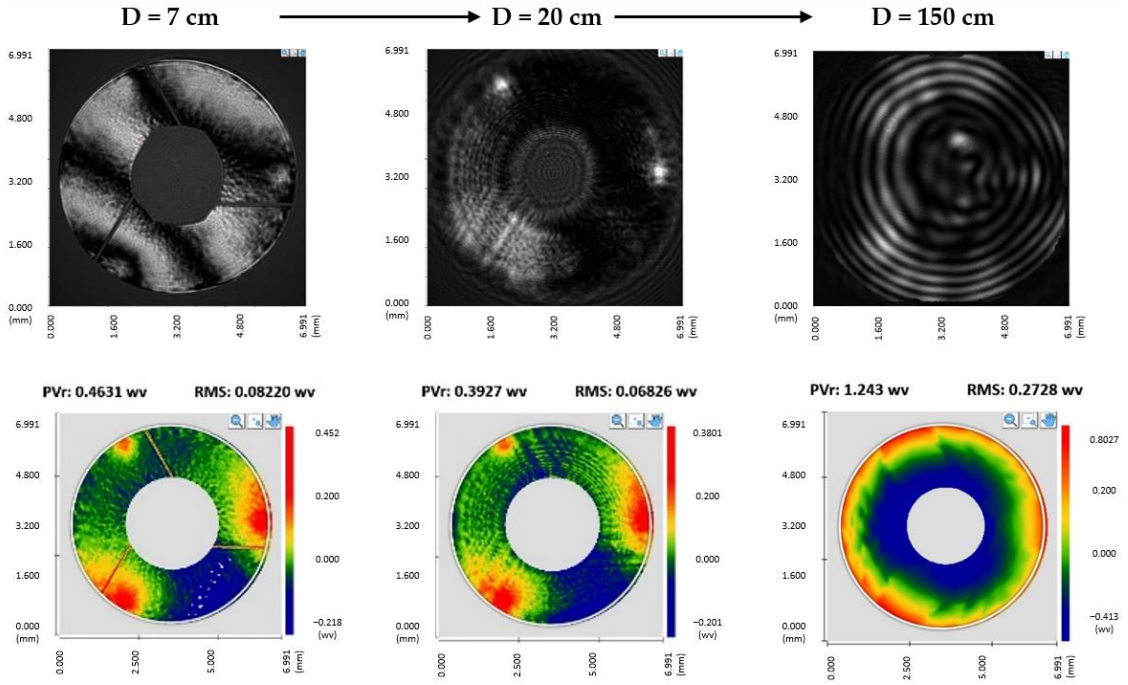

Figure 4. Separation distance D versus the interferogram and WFE map.

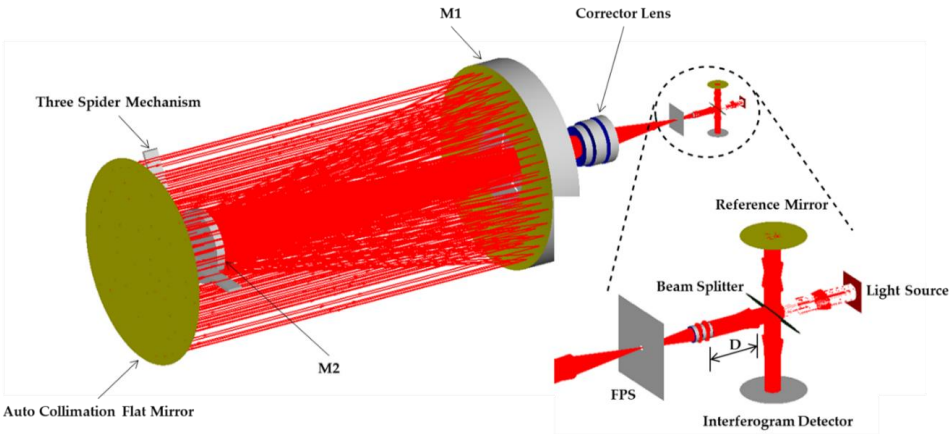

Figure 5. Double pass simulation model with the parametric separation distance D in ASAP.

The collimated beam produced by the light source would pass through the beam splitter and divide into two different optical paths. The first optical path is the reference beam from the internal flat of the interferometer where the second optical path is the object beam from the telescope reflected by the auto collimation flat mirror. The parameter of separation distance D increased from the nominal value of 7 cm to the final setup in the vacuum chamber of 150 cm in the simulation model. The fringe distribution of the interferogram is successfully obtained as shown in Figure 6, where the numbers of concentric fringes vary with the change of separation distance D. In addition, the obscuration of the

three spider mechanisms produces a diffraction pattern on the interferogram. The change of fringe number would affect the WFE calculation, especially for the power term of the Zernike coefficient and finally lead to a miscalculation of telescope defocus under the thermal vacuum circumstances.

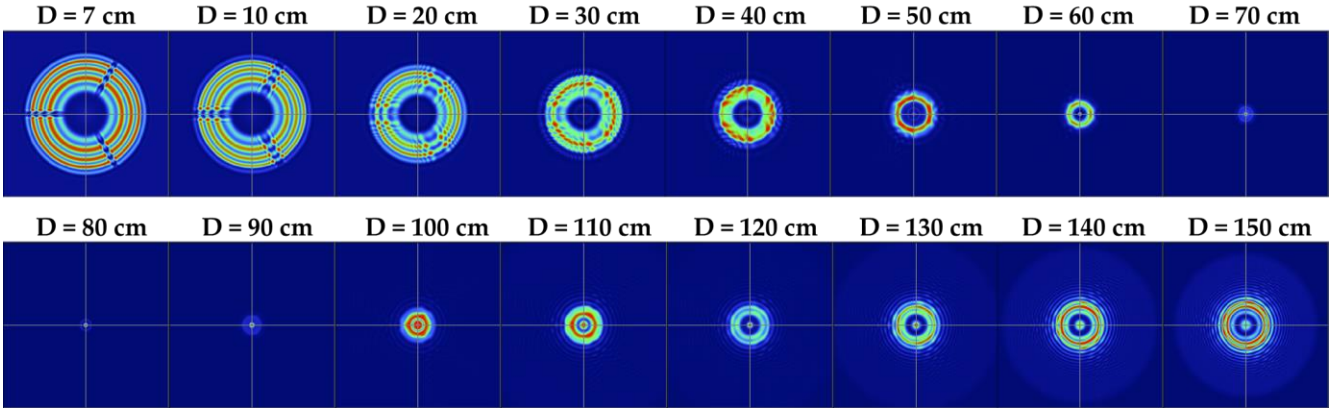

Figure 6. Fringe distribution of interferogram versus the separation distance D.

In addition, the double pass optical path was divided into two parts for investigating the major source of the blurry fringe. The first part is the collimated laser beam produced by the interferometer and the laser beam is assumed to have a Gaussian distribution with consideration of the 150 cm propagation distance. The calculation follows the beam waist formula as described in Equation (1):

$$w(z) = w_0\sqrt{1 + \left(\frac{\lambda z}{\pi {w_0}^2}\right)^2} \quad (1)$$

In Equation (1), w(z) represents the radius of the laser beam as a function of propagation distance (z) where the λ is the wavelength of the laser. Due to the diffraction effect, a Gaussian beam will converge to and diverge from the beam waist (w_0), which is the area where the beam diameter reaches a minimal value. The beam diameter varies by less than 0.01% based on the calculation of the beam waist formula, which means the collimated laser beam still remains in collimation after traveling through the 150 cm distance along the optical axis and could be excluded from the cause of the abnormal interferogram.

The second part is to analyze the object beam from the telescope as shown in Figure 7. A collimated light source was set in front of the telescope, which sequentially passes through the telescope and diverger lens and then finally reaches the interferogram detector. Figure 8 shows the fringe distribution, where the beam size would be varied with the separation distance, which implies the laser beam became un-collimated after passing through the diverger lens.

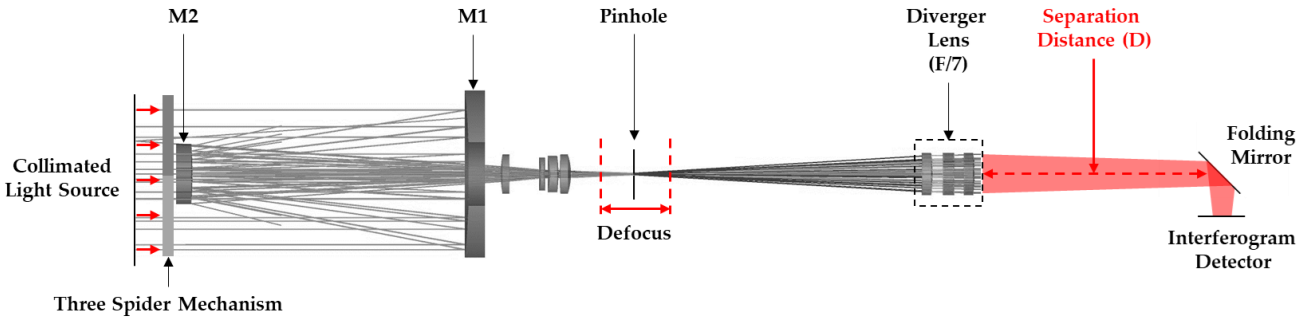

Figure 7. Simulation model of object beam from telescope.

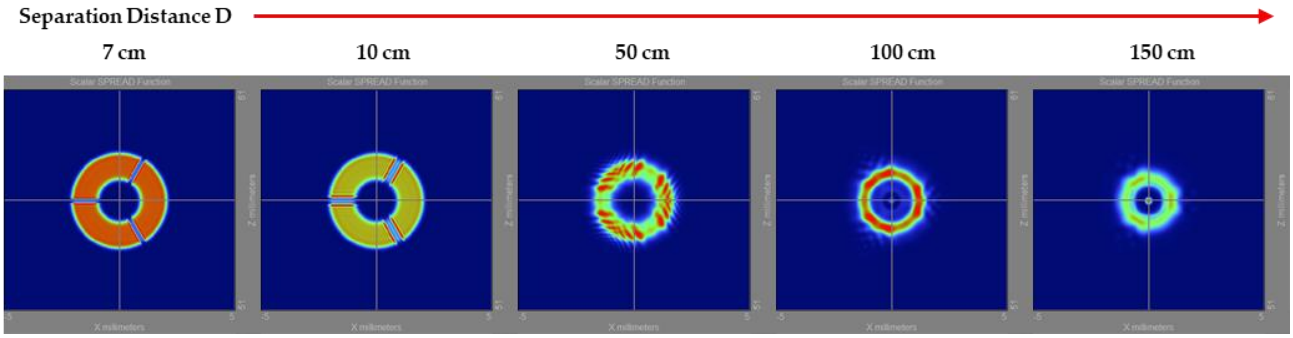

Figure 8. Simulation result of object beam from telescope.

The un-collimated result is related to the defocus between the telescope focal plane and diverger lens and the geometrical schematic of defocus versus beam size is shown in Figure 9. In our measurement architecture, if the defocus exceeds 100 um during the testing, the beam size on the interferogram would approximately increase over 1 mm in radius through the 150 cm propagation distance, which may converge to a smaller area before reaching the interferogram or diverge to exceed the active area of the interferogram detector.

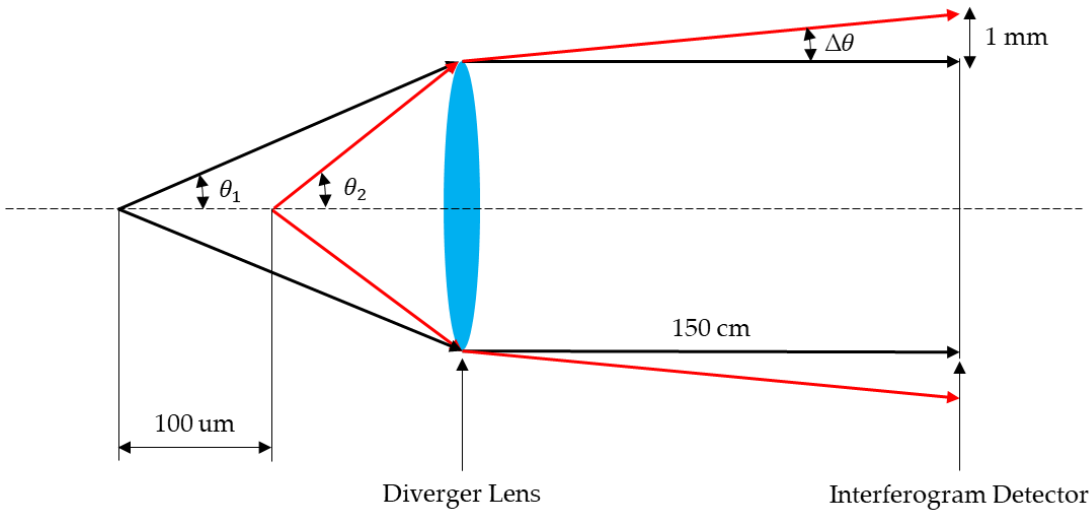

Figure 9. Geometrical schematic of defocus versus propagated beam size.

Even under an in focus condition, the diffraction caused by the three spider mechanism, which obscured the aperture of the telescope, still affected the fringe distribution while increasing the separation distance D as illustrated in Figure 10. As a result, the blurry fringe on the interferogram can be attributed to the combination of un-collimation of the returned beam from telescope and the diffraction effect of the spider mechanism.

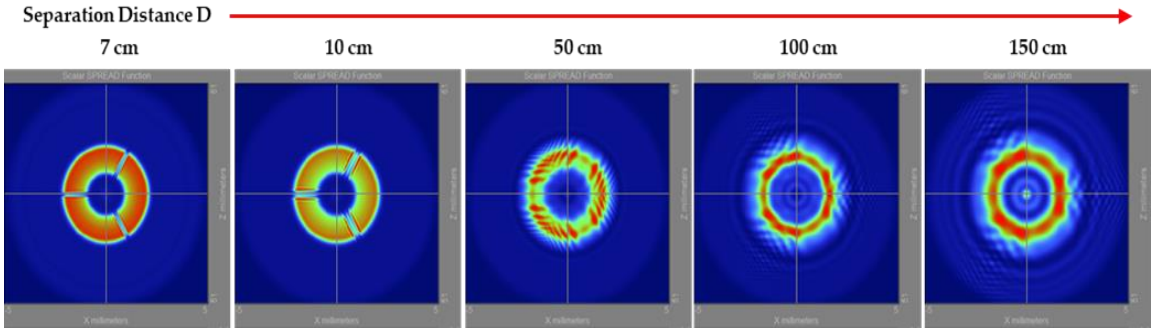

Figure 10. Diffraction effect of spider mechanism versus the separation distance.

The main purpose of the optical thermal vacuum test is to observe the defocus of the telescope under the space environment. Therefore, a solution for reducing the sensitivity of the un-collimated beam versus the defocus and diffraction effect of the mechanism becomes essential. Two approaches, including introducing relay optics and redesigning the opto-mechanical interface of the vacuum view port, are proposed to resolve the issue.

A relay optics can shift the focus range of the system to the spatial location with convenience. For resolving the large separation distance issue of the diverger lens, the first approach is to adopt a relay optics placed at the location between the diverger lens and the interferometer. A conceptual relay optics consisting of two lenses with a symmetrical design was added into the simulation in order to capture and reproduce the collimated beam along the optical path as illustrated in Figure 11.

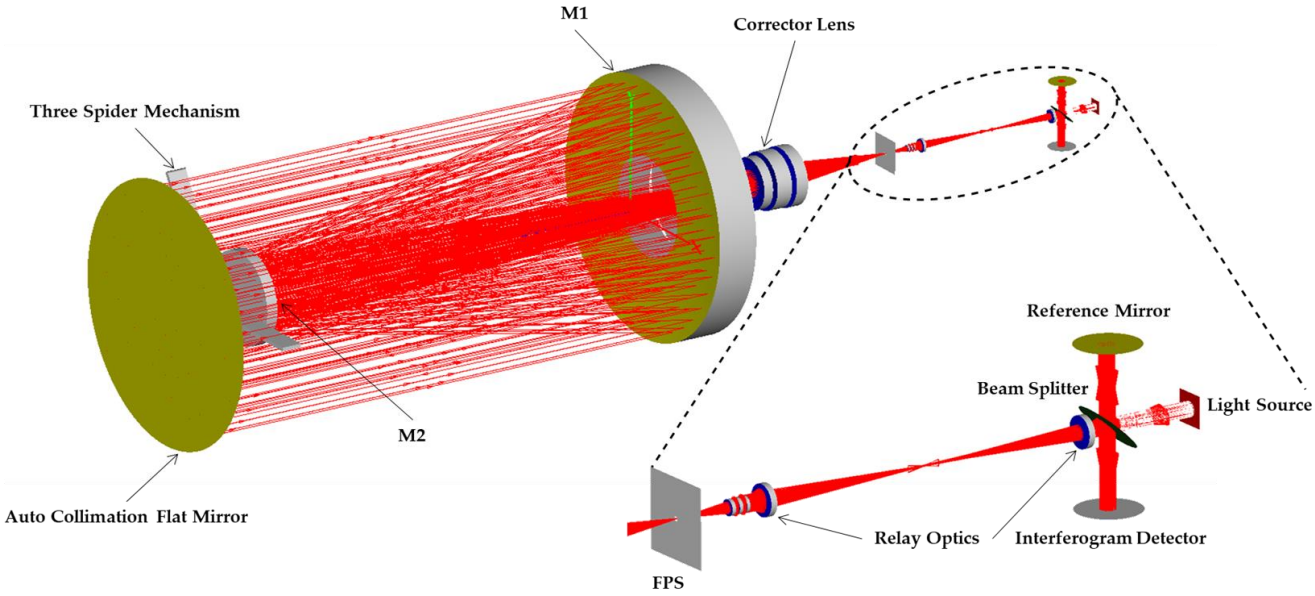

Figure 11. Simulation model for interferometric system with relay optics.

Figure 12 shows the simulation results, which indicate that the fringe distribution became insensitive to the change of the separation distance D after introducing the relay optics. For comparison, the fringe with relay optics at the separation distance D of 150 cm is similar to that of the case at separation distance D of 7 cm without relay optics as shown in Figure 13. Nevertheless, there remains a diffraction effect from the three spider mechanism. In addition, introducing relay optics would need another hexapod and more reference tools for the alignment, which would increase the complexity of the entire test setup.

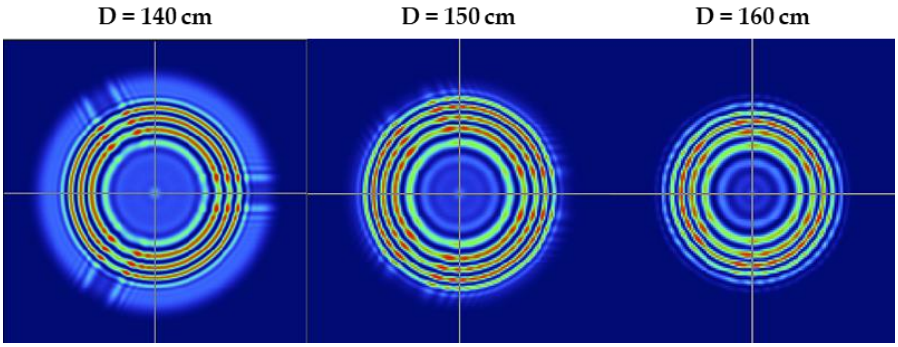

Figure 12. Simulated fringe distribution of separation distance variation with the addition of a relay lens.

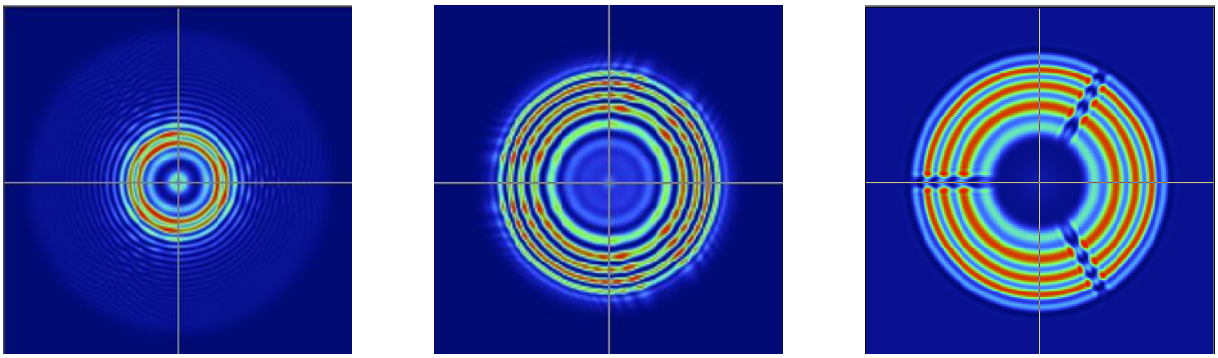

(**a**) (**b**) (**c**)

Figure 13. Comparison of simulated fringe distribution. (**a**) Fringe of 150 cm separation distance case without relay optics. (**b**) Fringe of 150 cm separation distance case with relay optics. (**c**) Fringe of 7 cm separation distance case.

Another approach is a more efficient way and allows for catching up with the tight schedule of the satellite project by modifying the mechanical structure of the vacuum view port of the chamber door. A 1.5 m long metallic tube structure with a high surface quality transmission flat was implemented on the rear side as a new vacuum view port for the purpose of shortening the separation distance D as illustrated in Figure 14a,b. In addition, the transmission flat was intentionally designed with a tilt angle to avoid the ghost fringe from its own two surfaces entering the interferometer.

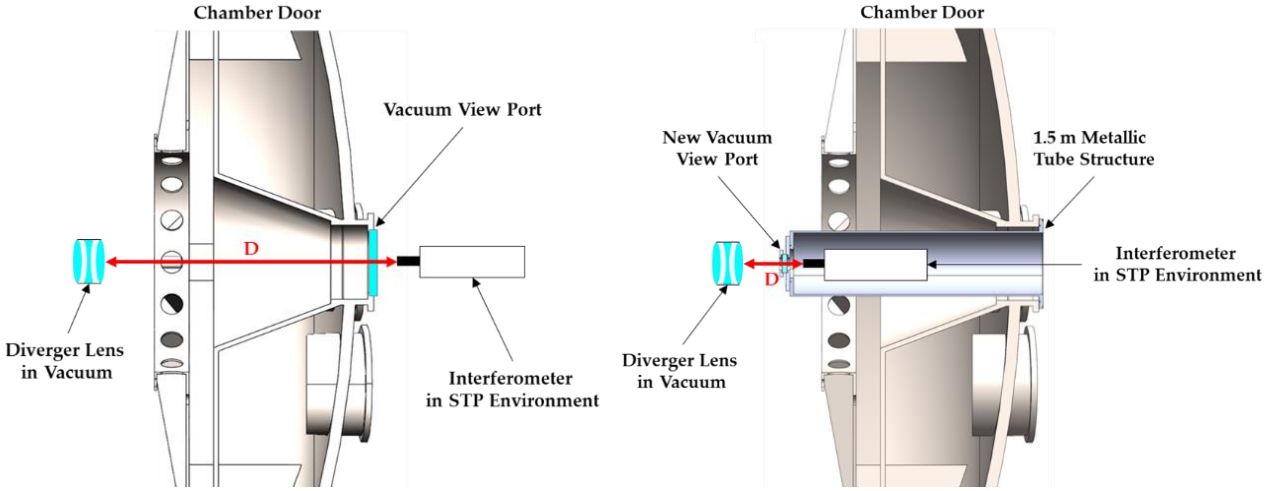

(**a**) (**b**)

Figure 14. Mechanical structure modification of the chamber door. (**a**) Original vacuum view port. (**b**) New vacuum view port.

Figure 15 shows the actual measurement setup in a vacuum chamber with the improved vacuum view port. Inside the chamber, all of the optical ground support equipment (OGSE), including the testbed, two vacuum compatible hexapods, auto collimation flat mirror and diverger lens were covered by the multi-layer insulation (MLI) material for stabilizing the temperature of the OGSE and minimizing the WFE fluctuation caused by the thermal deformation, as shown in Figure 15a. However, the telescope was bare without any thermal protection in order to investigate the optical performance degradation under the on orbit thermal cycling environment. On the other hand, the interferometer with its hexapod was placed outside the chamber and could reach the position close to the new vacuum view port by introducing a mechanical guide rail as shown in Figure 15b.

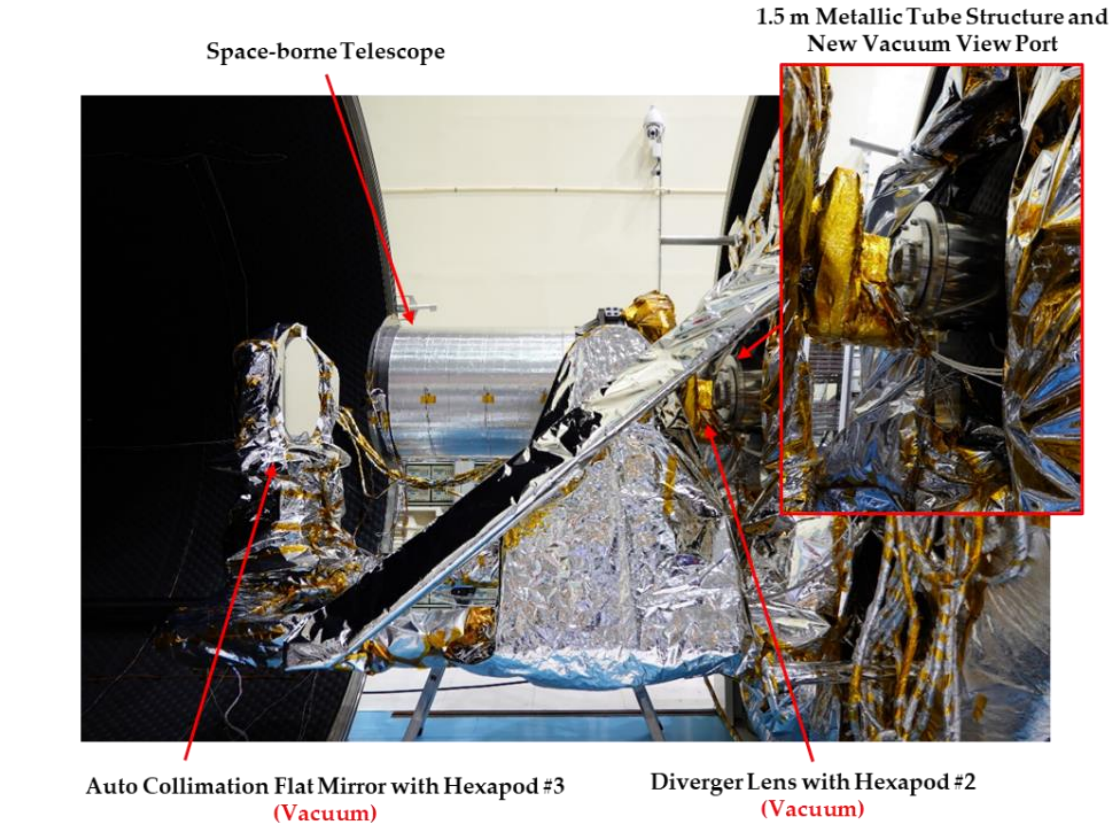

(**a**)

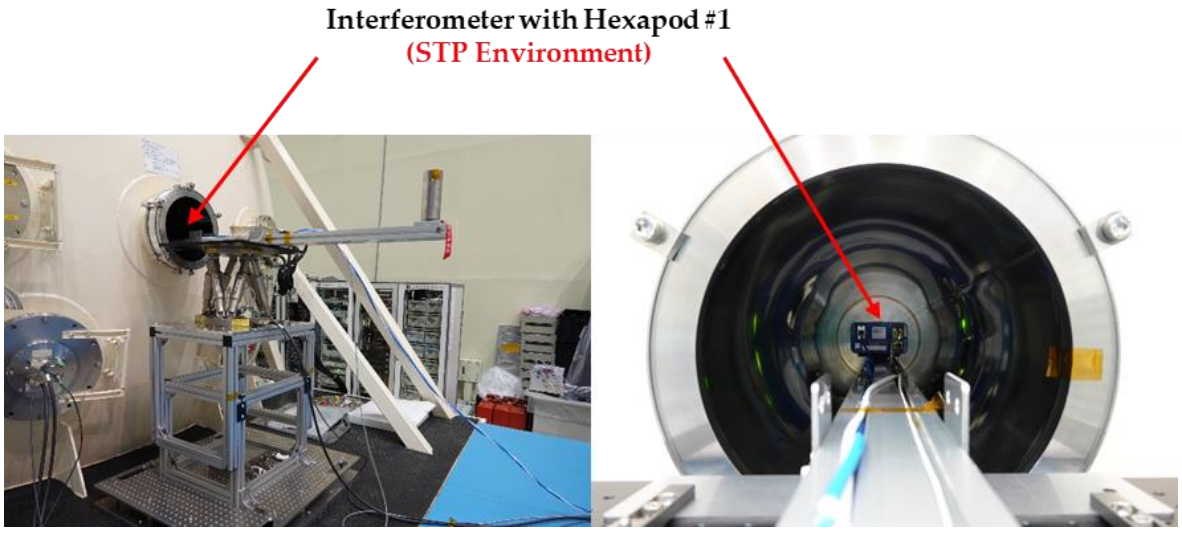

(**b**)

Figure 15. Improved measurement setup. (**a**) Measurement setup in thermal vacuum chamber. (**b**) Interferometer in STP environment.

4. Alignment Procedure for Interferometric Measurement

After resolving the major obstacle above, the next challenge was to align the diverger lens in the chamber without a firsthand look at the reflected spotlight. Figure 2 shows the double pass interferometry setup in the vacuum chamber and the two reference optics—focal plane simulator (FPS) and an alignment cube designed with a polished optical surface—that were placed on the focal plane of the telescope and nearby the diverger lens, respectively. For the alignment process, firstly, the collimated beam coming from the interferometer without a diverger lens projects to the 1st optical surface of the FPS. Then,

the reflected beam from the 1st optical surface returns to the interferometer and the auto collimation can be achieved as illustrated in Figure 16a. The position of the interferometer can be manipulated by the 1st hexapod in Figure 2 for the purpose of eliminating the centering and tilting error. The simulated interferogram before alignment with the tilt fringe and decenter error is shown in Figure 16b, where the result after alignment presents the null out fringe distribution as shown in Figure 16c.

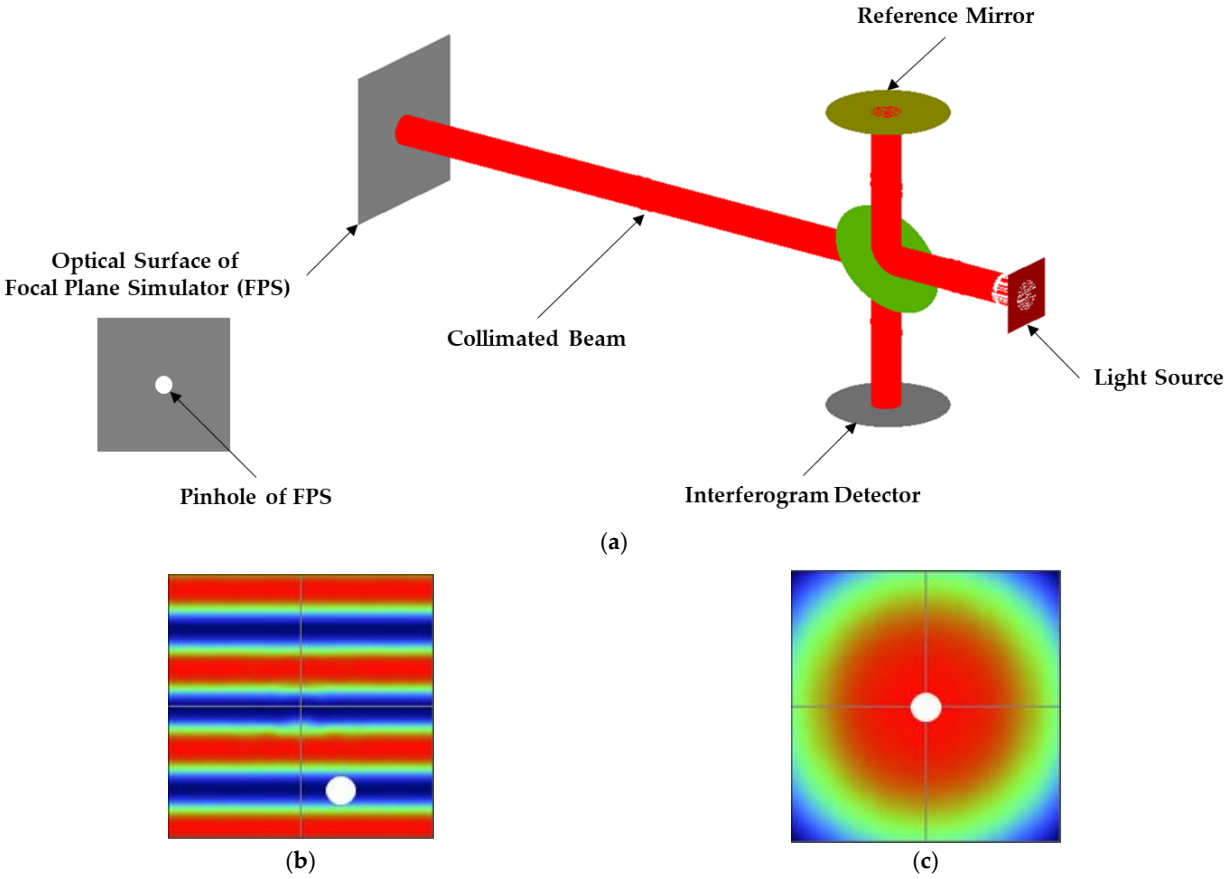

Figure 16. Alignment process of telescope and interferometer. (**a**) Alignment scheme of telescope and interferometer. (**b**) Interferogram with tilt and decenter. (**c**) Interferogram without tilt and decenter.

The second step is to align the diverger lens with the pre-aligned interferometer. The alignment cube and diverger lens are well aligned by the coordinate measurement machine (CMM), which could achieve a resolution better than 4 um under a 700 mm travel distance and was installed on the 2nd hexapod in advance as illustrated in Figure 2. The auto collimation between the 2nd optical surface of the alignment cube and interferometer could be achieved by tuning the tip tilt angle of the 2nd hexapod as in Figure 2 and the alignment diagram is the same as in Figure 16a. After that, by adjusting the 2nd hexapod along the optical axis direction, the focal point of the diverger lens can be located on the 1st optical surface, which is called the cat's eye position, as shown in Figure 17a. Figure 17b,c illustrate the interferogram before and after the focusing, respectively. The centering position of the diverger lens can be established by recording the lateral coordinates of the 2nd hexapod while the cats' eye focus vanishes due to the central pinhole of the FPS. Finally, the object beam from the telescope can be observed on the interferogram by adjusting the tip tilt angle of the auto collimation flat mirror using the 3rd hexapod as illustrated in Figure 2. The entire double pass setup in the vacuum chamber is completed at the end.

Combining the improved measurement setup and the rigorous alignment procedure, we could finally obtain the interferogram with modulation over 80% and a real time WFE result close to the nominal usage of the interferometer in the chamber as shown in Figure 18.

In addition, the WFE measurement budget is shown in Table 1, which illustrates the error contributors of the interferometry such as hexapod accuracy, vacuum transition of auxiliary optics, thermal control accuracy and vibration of the vacuum chamber, where the total RMS WFE accuracy is 10.5 nm, which is estimated by the root-sum-square (RSS) of each contributor. The telescope tolerance analysis was performed without including any compensator, i.e., the position of all of the components were located at the position as designed, including the FPA. In the analysis, the minimum MTF of 0.25 at the spatial frequency of 71.429 lp/mm was set as the criteria. The analyzed result illustrates the specified optical surface decenter error, tilt error and system RMS WFE, which will be able to meet all of the required tolerances [6].

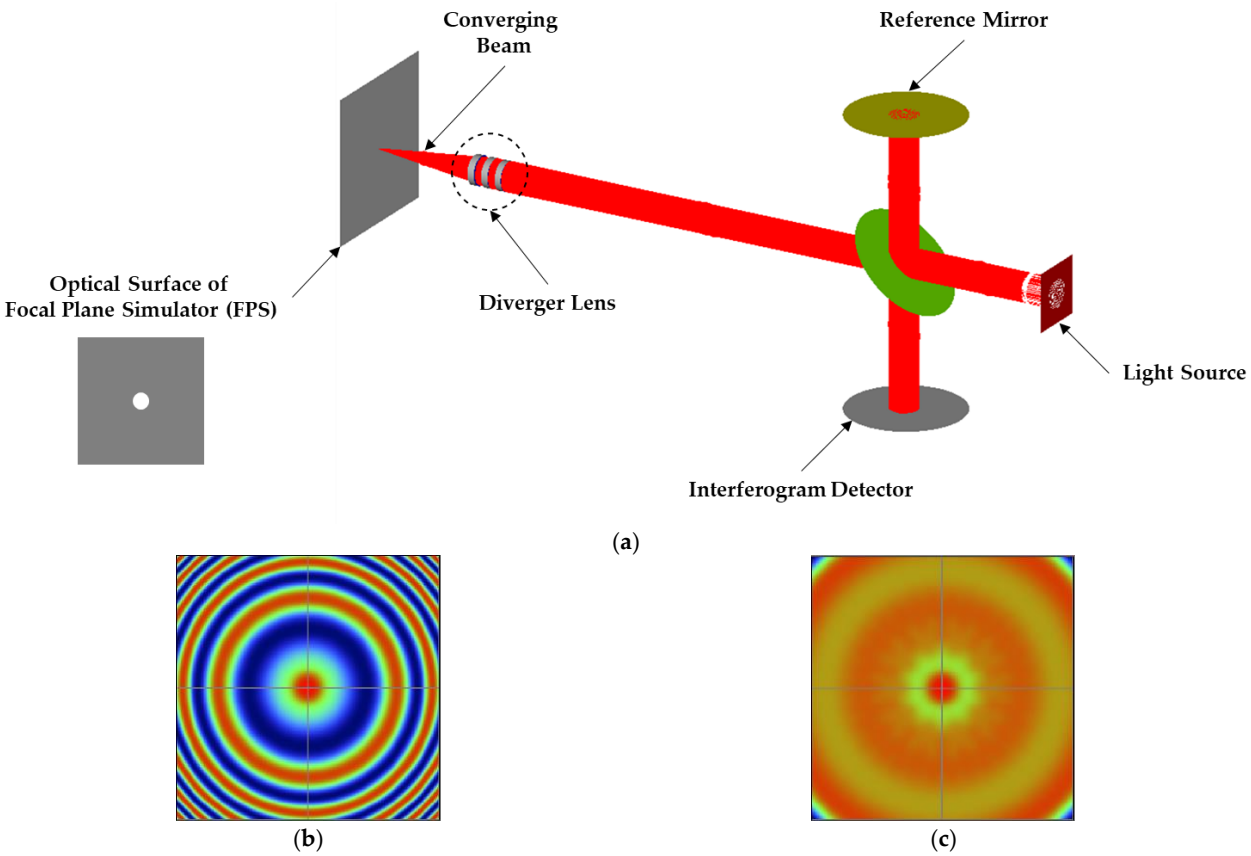

Figure 17. Alignment process of telescope and diverger lens. (**a**) Alignment of telescope and diverger lens with cat's eye position. (**b**) Interferogram with defocus. (**c**) Interferogram without defocus.

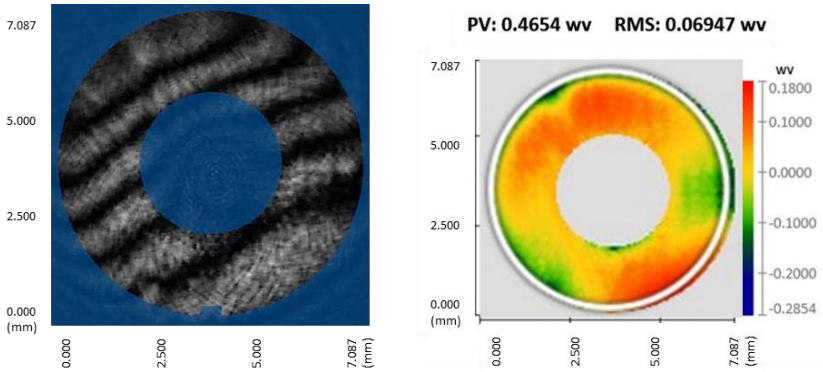

Figure 18. Interferogram and WFE map of the telescope under thermal vacuum circumstances.

Table 1. WFE measurement budget.

Contributors	Accuracy (RMS WFE nm)	Description
Interferometer hexapod accuracy	1.2 nm	Translation +/−0.5 µm, Rotation +/−9 µrad
Diverger lens hexapod accuracy	2.0 nm	Translation +/−0.15 µm, Rotation +/−3 µrad
Auto collimation flat hexapod accuracy	1.3 nm	Translation +/−0.5 µm, Rotation +/−9 µrad
Vacuum transition	1.5 nm	$<10^{-5}$ mbar
Thermal control accuracy	4.5 nm	+/−0.2 °C
Vacuum chamber vibration criteria	9.0 nm	VC-C
Total WFE accuracy	10.5 nm	RSS of all contributors

Moreover, the telescope optical performance under the thermal vacuum environment was also successfully acquired, including the focus shifting due to the vacuum transition of the CFRP Tube structure and thermal cycling condition. Figure 19 shows the moisture effect that would cause a significant focus change with a large slope within 24 h and finally became stable over 48 h under a high vacuum level circumstance. For the thermal cycling test, the repeatability of the focus performed well after four iterations as shown in Figure 20 despite the telescope being bare without MLI protection, which gave us more confidence because the flying model of the telescope would be implemented with precise temperature control.

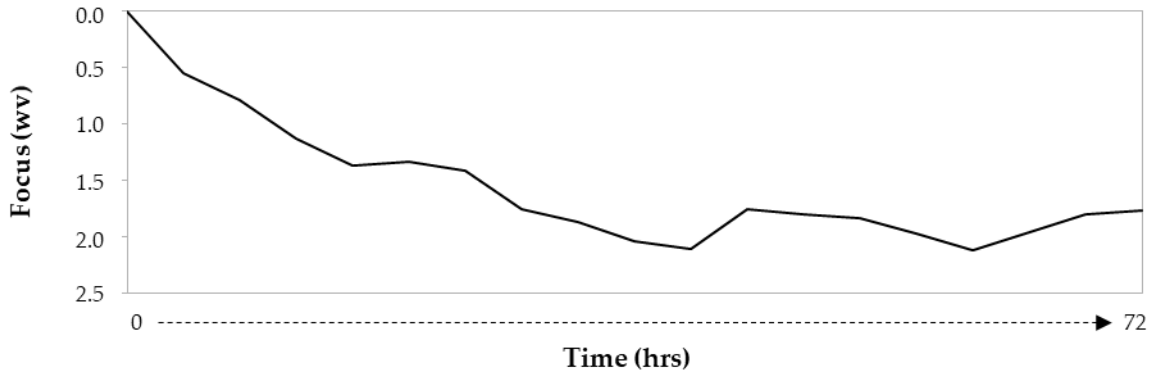

Figure 19. Focus term variation with time under high vacuum level circumstances.

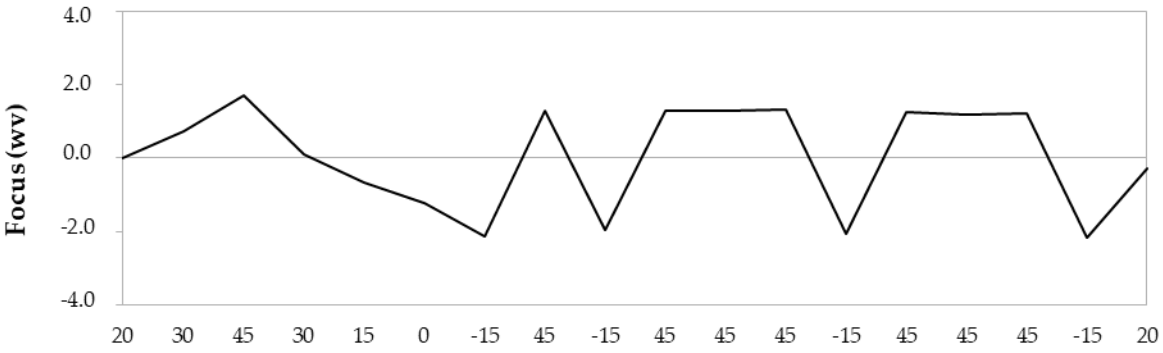

Figure 20. Focus term variation with temperature under thermal cycling conditions.

5. Conclusions

The proposed measurement architecture overcomes the difficulties of testing a large aperture optical system in a vacuum chamber with a narrow internal space and vacuum view port with a limited aperture size. The most valuable part of this study is that the focus change of a space-borne telescope could be obtained under a thermal vacuum circumstance before the image sensor is installed, which could avoid any reassembly work. The variation of the interference fringe due to the relocation of the diverger lens has been resolved by the modification of the vacuum viewport. In addition, all of the involved optics could successfully align with the measuring instrument without a firsthand look at the spotlight through the developed optical alignment procedure and specially designed reference tools. The total WFE measurement accuracy is 10.5 nm RMS WFE, with consideration of the error contributors of the testbed. Furthermore, despite the measurement being accomplished on a Twyman–Green type interferometer, a similar concept can be applied to other types of interferometers due to their similar interferometric light path.

Author Contributions: Conceptualization, Y.-K.H.; methodology, Y.-K.H.; software, Y.-K.H.; validation, Y.-K.H.; formal analysis, Y.-K.H.; investigation, Y.-K.H.; data curation, Y.-K.H.; writing—original draft preparation, Y.-K.H.; writing—review and editing, C.-H.C.; visualization, Y.-K.H.; supervision, C.-H.C. All authors have read and agreed to the published version of the manuscript.

Funding: This research received no external funding.

Institutional Review Board Statement: Not applicable.

Informed Consent Statement: Not applicable.

Data Availability Statement: Data is unavailable due to privacy or ethical restrictions.

Acknowledgments: I would like to express my thanks to Po-Hsuan Huang from the Taiwan Space Agency for supporting the resources for the experiment and the discussions of developing the ideas put forward here. The success of this research is attributed to his invaluable advice.

Conflicts of Interest: The authors declare no conflict of interest.

Abbreviations

STP	Standard Temperature and Pressure
CFRP	Carbon Fiber Reinforced Polymer
NISP	Near Infrared Spectrometer and Photometer
SHWFS	Shack–Hartmann Wavefront Sensor
M1	Primary Mirror
M2	Secondary Mirror
WFE	Wavefront Error
ASAP	Advanced Systems Analysis Program
OGSE	Optical Ground Support Equipment
MLI	Multi-Layer Insulation
FPS	Focal Plane Simulator
CMM	Coordinate Measurement Machine
VC	Vibration Criteria
RSS	Root-Sum-Square

References

1. Yoder, P. *Opto-Mechanical Systems Design*, 3rd ed.; Taylor & Francis: Boca Raton, FL, USA, 2006.
2. Baxter, E.; Levett, B. *TopSat: Lessons Learned from a Small Satellite Mission, Small Satellites for Earth Observation*; Springer: Dordrecht, The Netherlands, 2008; pp. 377–384.
3. Bodendorf, C.; Geis, N.; Grupp, F.; Kaminski, J.; Katterloher, R.; Bender, R. Testing the near-infrared optical assembly of the space telescope Euclid. In Proceedings of the SPIE Optical Engineering + Applications, San Diego, CA, USA, 11–15 August 2019.
4. Gloesener, P.; Wolfs, F.; Cola, M.; Pirnay, O.; Flebus, C. Euclid mirrors and test collimator: AMOS developments. In *Advances in Optical and Mechanical Technologies for Telescopes and Instrumentation II*; SPIE Astronomical Telescopes + Instrumentation: Edinburgh, UK, 2016; Volume 9912.

5. Liébecq, S.; Tychon, I.; Jacques, L.; Marquet, B.; Lallemand, E.; Samain, V.; Kellens, A.; Grodent, C.; Martin, Y.; Saltalamaccia, N.; et al. Euclid payload module: Thermal balance and thermal vacuum test at csl premises. In Proceedings of the 17th ECSSMET, Toulouse, France, 28–30 March 2023.
6. Lin, S.-F.; Chen, C.-H.; Huang, Y.-K. Optimal F-Number of Ritchey–Chrétien Telescope Based on Tolerance Analysis of Mirror Components. *Appl. Sci.* **2020**, *10*, 5038. [CrossRef]
7. Shiefman, J. Shiefman Consulting, Using Software to Model Coherent Metrology Systems. In Proceedings of the SPIE Vol. 5174 Novel Optical Systems Design and Optimization V, Bellingham, WA, USA, 3–8 August 2003.
8. Douglas, N.G.; Jones, A.R.; van Hoesel, F.J. Ray-based simulation of an optical interferometer. *Opt. Soc. Am. A* **1995**, *12*, 124–131. [CrossRef]
9. Harvey, J.E.; Irvin, R.G.; Crabtree, K.; Pfisterer, R.N.; Breckinridge, J.B. Diffraction analysis of large segmented mirror concepts for exoplanet exploration. In Proceedings of the Space Telescopes and Instrumentation 2018: Optical, Infrared, and Millimeter Wave, Austin, TX, USA, 10–15 June 2018; Volume 10698.